ChemComm

COMMUNICATION

View Article Online
View Journal | View Issue

Cite this: *Chem. Commun.*, 2025, **61**, 9468

Received 11th May 2025,
Accepted 21st May 2025

DOI: 10.1039/d5cc02677f

rsc.li/chemcomm

Mitigating X-ray-induced damage for accurate analysis of battery cathodes using transmission X-ray microscopy†

Muhammad Mominur Rahman,[a] Nan Wang,[a] Xianghui Xiao*[b] and Enyuan Hu*[a]

We investigate the impact of X-ray-induced damage on the evolution of battery cathodes using synchrotron transmission X-ray microscopy. In an *operando* coin cell, exposure to the X-ray beam can induce bubble formation, potentially rendering cathode particles electrochemically inactive and displacing particles from their initial position. However, utilizing external pressure on a pouch cell can mitigate bubble formation and its associated effects.

Probing beams such as electrons, neutrons, and X-rays, have revolutionized materials characterization, providing unprecedented insights into material properties and guiding the design and synthesis of improved functional materials.[1–4] Battery materials are a notable example, benefiting significantly from advanced characterization techniques that have contributed to the development of safer, higher-energy-density batteries.[5–7] Technological advancements, such as those enabled by synchrotron radiation facilities, have made it possible to study battery materials during operation, revealing their chemical, structural, and morphological evolution in real-time.[8–12] However, a key challenge in characterizing battery materials, particularly using *operando* techniques, is the potential for radiation-induced damage to battery components.[13–16] For instance, electrons in transmission electron microscopy have been reported to induce lattice structure changes in battery cathodes.[17] Similar radiation-induced lattice changes have also been observed in synchrotron studies.[18]

As the probing area in battery characterization is typically small, damage to particles within that area may not noticeably affect overall electrochemical performance. Consequently, while electrochemical data might appear consistent, the corresponding characterization results may fail to accurately represent the actual reaction mechanisms. Drawing conclusions based on damaged battery components can lead to significant errors and biased interpretations.[19]

This issue is particularly critical in synchrotron X-ray studies due to their high flux and intensity. To address beam-induced damage, careful consideration should be given to the exposure and flux of the probing beam as well as the *operando* cell setup in accordance with this study. Optimizing these parameters can mitigate damage and enable more representative and accurate characterization of battery components under investigation. While, X-ray energy is another key parameter, it is fixed by the element under investigation, allowing little room for modification.

Transmission X-ray microscopy (TXM) is a powerful technique for characterizing battery materials, providing high spatial resolution to analyze morphology and chemical distribution. When combined with *operando* setups, TXM has gained increasing popularity as an effective diagnostic tool to study various battery phenomena, including thermal runaway, fast charging, and lithium dendrite formation, among others.[8,20–23] In this work, we examine the impact of beam-induced damage during *operando* TXM characterization of battery materials and explore potential strategies to mitigate this effect.

We performed imaging at a specific energy of 8.4 keV to investigate bubble formation in the absence of battery cycling (Fig. 1b) and conducted 2D X-ray absorption near edge structure (XANES) imaging to study the impact of bubble formation on the chemical evolution of nickel in the $LiNi_{0.6}Mn_{0.2}Co_{0.2}O_2$ (NMC622) cathode material during battery cycling (Fig. 2).[24–27] These experiments were carried out at the full field X-ray imaging (FXI) beamline of NSLS-II.

The schematic of the imaging setup for *operando* battery studies at the FXI beamline is shown in Fig. 1a. The X-ray beam is focused onto a region of interest within the battery using a capillary condenser through a Kapton window. The transmitted X-ray beam forms a magnified image at the detector position through a zone plate lens. The detector consists of a CsI scintillator, a 10× Nikon optical objective lens, and an Andor Neo 5.5 sCMOS camera.

[a] *Chemistry division, Brookhaven National Laboratory, Upton, NY, 11973, USA. E-mail: enhu@bnl.gov*
[b] *National Synchrotron Light Source II, Brookhaven National Laboratory, Upton, NY, 11973, USA. E-mail: xiao@bnl.gov*

† Electronic supplementary information (ESI) available. See DOI: https://doi.org/10.1039/d5cc02677f

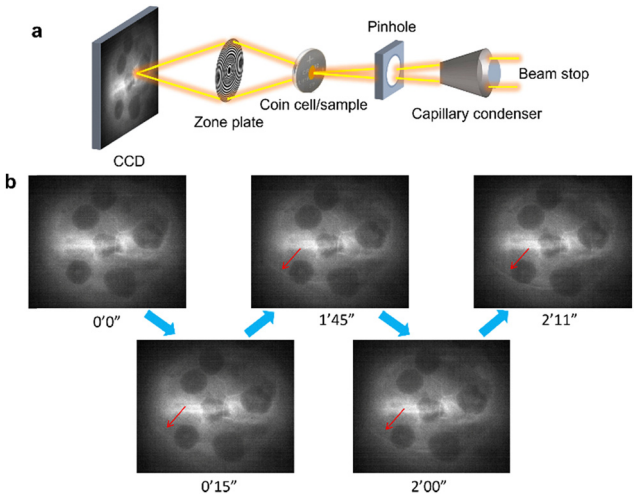

Fig. 1 Evidence of X-ray induced damage in battery materials. (a) Schematic illustration of the working mechanism of transmission X-ray imaging of *operando* battery setup. (b) Beam damage as evidenced by the bubble formation (red arrow) upon exposure of the X-ray transparent field of view of the *operando* coin cell to X-ray. X-ray energy was 8.4 keV and the flux was reduced to 7.8×10^6 photons per μm^2 s^{-1} by using attenuators, which is only 1% of the total available flux.

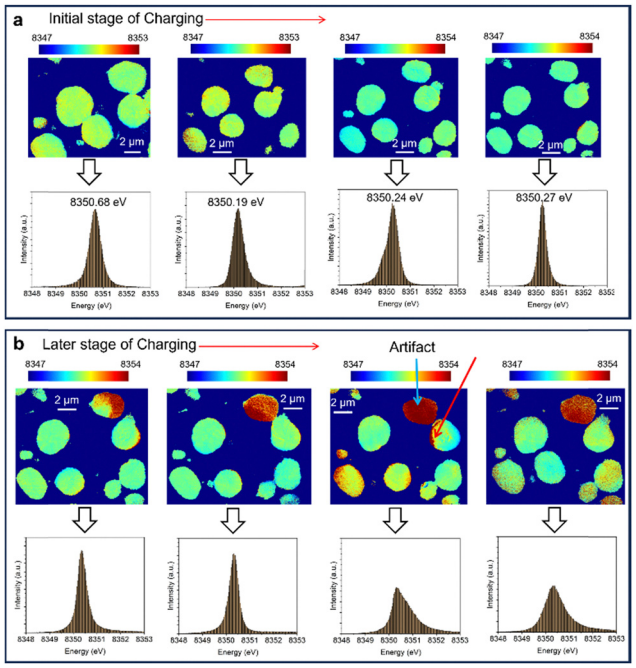

Fig. 2 Effect of beam damage on chemical evolution of battery cathode particles. *In situ* Ni 2D XANES map of NMC622 cathode particles (top row) and the corresponding histogram of energy distribution (bottom row). The images are collected during the first half of charging (a). Similar 2D XANES map and histogram for later half of charging is shown in (b). Cycling was performed at C/10 rate. Every map is taken 1 hour apart.

Fig. 1b displays raw 2D images of NMC622 particles within the field of view (FOV) without further processing. All images in Fig. 1b were acquired at 8.4 keV in a coin cell with a Kapton tape-covered hole to allow X-ray transmission. The battery remained at rest during image acquisition to isolate the effects of X-ray-induced damage from those of cycling. To minimize beam damage, the illumination beam flux was reduced to 7.8×10^6 photons per μm^2 s^{-1} using attenuators, corresponding to approximately 1% of the available flux. Despite the reduced dose, evidence of beam damage was observed, as bubbles appeared within the FOV shortly after the beam was turned on. With prolonged exposure, bubbles propagated further (marked by the red arrow in Fig. 1b).

We hypothesize that this bubble formation results from electrolyte decomposition induced by the probing X-ray beam.[16] The bubble formation phenomenon was consistently observed across multiple FOVs, as shown in Fig. S1 and S2 (ESI†), highlighting its recurring nature.

Bubble formation induced by beam damage can significantly influence the chemical evolution of transition metal elements in cathode particles. For instance, bubbles can disrupt the electrochemical connections between particles and the electrolyte, hindering the ion transport. This isolation may render some particles within the field of view (FOV) electrochemically inactive. However, since the FOV is relatively small (50 μm × 40 μm) compared to the entire electrode size (~12 mm), damage to selected particles under investigation may have minimal impact on the overall cycling performance.

To investigate the effects of beam damage, we acquired 2D-XANES images of nickel (Ni) to monitor its redox evolution in NMC622 during coin cell battery cycling. The images were fitted around the white-line energy of the Ni K-edge to estimate the redox evolution of Ni in NMC622. Image fitting was performed using the TXM-Sandbox software package.[28,29] Evidence of beam damage was apparent even at the start of cycling, as bubbles formed and propagated within the FOV during image collection (Fig. S3, ESI†).

Fitted 2D-XANES images reveal that during the initial hours of charging, no significant change in the Ni oxidation state is observed (Fig. 2a). The overall histogram of energy distribution shows no shift in the maximum, which correlates directly to the Ni oxidation state, indicating that Ni's oxidation state remains essentially unchanged. This conclusion holds even when analyzing smaller areas within individual cathode particles (Fig. S4, ESI†).

As charging progresses, beam damage accumulates, and bubble formation intensifies, potentially displacing particles from their initial positions (Fig. S5, ESI†). This particle movement can significantly impact image analysis. Accurate 2D-XANES fitting requires strict image reconstruction, which becomes challenging if particles move within the FOV, complicating reliable image alignment. Such displacement may introduce artifacts, such as the higher white-line energy observed at the edge of the particle marked by a red arrow in Fig. 2b.

Interestingly, the white-line energy of the particle marked by the blue arrow in Fig. 2b gradually increases during charging, while other particles show no significant changes. This suggests that bubble formation does not affect all particles uniformly. The particle marked by the red arrow in Fig. 2b appears

to remain electrochemically connected to the electrolyte and current collector, allowing redox reactions to continue in this specific particle. Radiation-induced artifacts like these can skew conclusions drawn from image analysis. Therefore, careful consideration must be given to analyzing particles subjected to beam damage to ensure reliable results.

We hypothesize that bubble formation and beam damage effects can be mitigated, to some extent, by applying external pressure to the cell. External pressure may suppress bubble formation and help maintain the electrochemical activity of the particles. A pouch cell configuration is particularly suitable for applying such pressure. To test this hypothesis, we assembled pouch cells with a $Li_{1.2}Ni_{0.15}Co_{0.1}Mn_{0.55}O_2$ cathode[8,22] and a lithium metal anode for *operando* transmission X-ray microscopy imaging (Fig. 3a).

The pouch cell was sandwiched between two steel plates to apply external pressure (Fig. 3b). These plates feature narrow open slots in the center to allow X-ray transmission.[30] Pouch cells are better suited for applying external pressure than rigid coin cells. Additionally, the design of the *operando* coin cell-featuring holes covered with Kapton tape may result in inhomogeneous pressure distribution across the cell during cell assembly, with reduced pressure in the X-ray transparent regions. In the pouch cell, the X-ray beam penetrates through the polymer housing, lithium metal anode, separator, and cathode. Using beam energy near the transition metal K-edge, such as the Ni K-edge, we could visualize cathode particles without interference from other battery components. The cell was charged at a C/2 rate, and images were collected every 30 minutes.

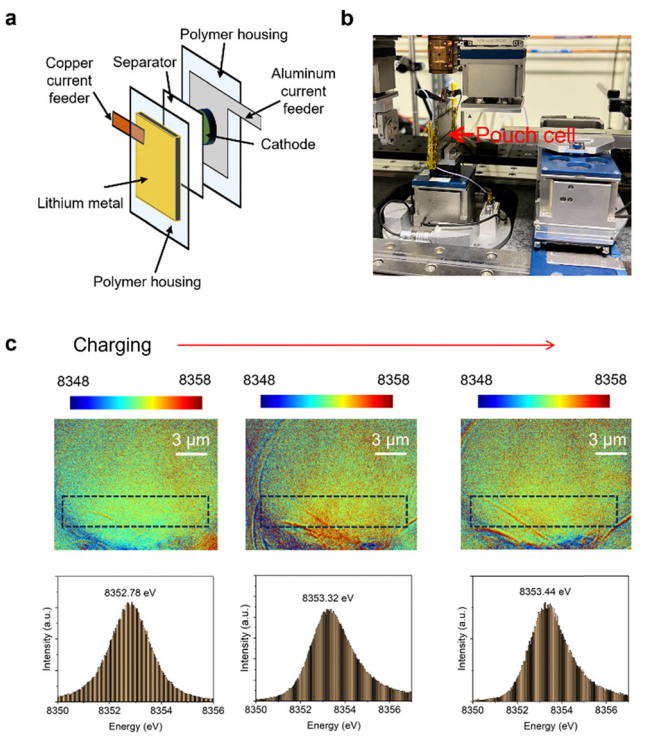

Fig. 3 Alleviation of beam damage through employing pouch cell setup for *operando* analysis. (a) and (b) Pouch cell setup for *operando* battery cycling for transmission X-ray microscopy imaging. (c) Ni 2D-XANES collected from the cycling of the pouch cell. The boxed region shows the area where the histogram analysis was performed.

Histogram analysis of the white-line energy distribution in the Ni 2D-XANES maps demonstrates that the redox reaction of Ni can be effectively captured in this setup (Fig. 3c). A blue shift in the Ni white-line energy was observed upon charging, confirming the ability to track the oxidation state of Ni under these conditions. These results suggest that applying pressure can help reduce beam damage effects.

However, the observed shift in the Ni K-edge white-line energy was smaller than expected, indicating that the mitigation of beam damage was not fully achieved.[8] This suggests that more precise control and tuning of the applied pressure may be necessary to further minimize beam damage and its associated effects efficiently. Previous studies have indicated that the extent of the applied pressure may influence the electrochemical performance in Li-ion cells and Li metal deposition morphology in Li metal cells.[31,32] Varying the pressure may have similar effect on mitigating the bubble formation. Further studies may involve including pressure control device in the *operando* cell setup and varying the extent of the pressure to create a correlation between pressure and bubble formation. However, as a proof concept, this study showcases the benefits of applying external pressure to mitigating bubble formation and beam damage effects.

In summary, we demonstrate the impact of X-ray-induced damage on *operando* analysis of battery cathodes using transmission X-ray microscopy. Beam damage can result in bubble formation within the exposed field of view (FOV), leading to particle deactivation and displacement. This effect can be mitigated by applying external pressure to the cell, with pouch cells being particularly well-suited for this purpose. Conducting *operando* experiments on pouch cells reduces beam damage, allowing for the observation of regular chemical changes in cathode particles during battery cycling.

The work done at BNL is supported by the Assistant Secretary for Energy Efficiency and Renewable Energy (EERE), Vehicle Technology Office (VTO) of the US Department of Energy (DOE) through the Advanced Battery Materials Research (BMR) Program under contract no. DE-SC0012704. This research used 18-ID (FXI) beamline of the National Synchrotron Light Source II, US DOE Office of Science User Facilities operated for the DOE Office of Science by BNL under contract no. DE-SC0012704.

Data availability

Data for this article is available at figshare at **https://doi.org/10.6084/m9.figshare.27891210**.

Conflicts of interest

There are no conflicts to declare.

Notes and references

1 Z. Shadike, H. Lee, O. Borodin, X. Cao, X. Fan, X. Wang, R. Lin, S.-M. Bak, S. Ghose and K. Xu, *Nat. Nanotechnol.*, 2021, **16**, 549–554.
2 M. J. Zachman, Z. Tu, S. Choudhury, L. A. Archer and L. F. Kourkoutis, *Nature*, 2018, **560**, 345–349.
3 S. Tan, J.-M. Kim, A. Corrao, S. Ghose, H. Zhong, N. Rui, X. Wang, S. Senanayake, B. J. Polzin and P. Khalifah, *Nat. Nanotechnol.*, 2023, **18**, 243–249.
4 E. Hu, Q. Li, X. Wang, F. Meng, J. Liu, J.-N. Zhang, K. Page, W. Xu, L. Gu and R. Xiao, *Joule*, 2021, **5**, 720–736.
5 F. Lin, Y. Liu, X. Yu, L. Cheng, A. Singer, O. G. Shpyrko, H. L. Xin, N. Tamura, C. Tian and T.-C. Weng, *Chem. Rev.*, 2017, **117**, 13123–13186.
6 D. Liu, B. Wu, Y. Xu, J. Ellis, A. Baranovskiy, D. Lu, J. Lochala, C. Anderson, K. Baar and D. Qu, *Nat. Energy*, 2024, **9**, 559–569.
7 S.-M. Bak, E. Hu, Y. Zhou, X. Yu, S. D. Senanayake, S.-J. Cho, K.-B. Kim, K. Y. Chung, X.-Q. Yang and K.-W. Nam, *ACS Appl. Mater. Interfaces*, 2014, **6**, 22594–22601.
8 E. Hu, X. Yu, R. Lin, X. Bi, J. Lu, S. Bak, K.-W. Nam, H. L. Xin, C. Jaye and D. A. Fischer, *Nat. Energy*, 2018, **3**, 690–698.
9 M. M. Rahman, A. Ronne, N. Wang, Y. Du and E. Hu, *ACS Energy Lett.*, 2024, **9**, 2024–2030.
10 S. Tan, Z. Shadike, J. Li, X. Wang, Y. Yang, R. Lin, A. Cresce, J. Hu, A. Hunt and I. Waluyo, *Nat. Energy*, 2022, **7**, 484–494.
11 J. A. Lewis, F. J. Q. Cortes, Y. Liu, J. C. Miers, A. Verma, B. S. Vishnugopi, J. Tippens, D. Prakash, T. S. Marchese and S. Y. Han, *Nat. Mater.*, 2021, **20**, 503–510.
12 D. P. Finegan, M. Scheel, J. B. Robinson, B. Tjaden, I. Hunt, T. J. Mason, J. Millichamp, M. Di Michiel, G. J. Offer and G. Hinds, *Nat. Commun.*, 2015, **6**, 6924.
13 A. P. Black, C. Escudero, F. Fauth, M. Fehse, G. Agostini, M. Reynaud, R. G. Houdeville, D. Chatzogiannakis, J. Orive and A. Ramo-Irurre, *Chem. Mater.*, 2024, **36**, 5596–5610.
14 R. Fantin, A. Van Roekeghem, J. P. Rueff and A. Benayad, *Surf. Interface Anal.*, 2024, **56**, 353–358.
15 R. Qiao, Y.-D. Chuang, S. Yan and W. Yang, *PLoS One*, 2012, **7**, e49182.
16 C. Tan, D. J. Lyons, K. Pan, K. Y. Leung, W. C. Chuirazzi, M. Canova, A. C. Co and L. R. Cao, *J. Power Sources*, 2016, **318**, 242–250.
17 F. Lin, I. M. Markus, M. M. Doeff and H. L. Xin, *Sci. Rep.*, 2014, **4**, 5694.
18 T. Jousseaume, J.-F. Colin, M. Chandesris, S. Lyonnard and S. Tardif, *ACS Energy Lett.*, 2023, **8**, 3323–3329.
19 M. Li, W. Liu, D. Luo, Z. Chen, K. Amine and J. Lu, *ACS Energy Lett.*, 2022, **7**, 577–582.
20 M. Vahnstiege, M. Winter, S. Nowak and S. Wiemers-Meyer, *Phys. Chem. Chem. Phys.*, 2023, **25**, 24278–24286.
21 W. Zuo, J. Gim, T. Li, D. Hou, Y. Gao, S. Zhou, C. Zhao, X. Jia, Z. Yang and Y. Liu, *Nat. Nanotechnol.*, 2024, 1–10.
22 J. Zhang, Q. Wang, S. Li, Z. Jiang, S. Tan, X. Wang, K. Zhang, Q. Yuan, S.-J. Lee and C. J. Titus, *Nat. Commun.*, 2020, **11**, 6342.
23 J. Li, N. Sharma, Z. Jiang, Y. Yang, F. Monaco, Z. Xu, D. Hou, D. Ratner, P. Pianetta and P. Cloetens, *Science*, 2022, **376**, 517–521.
24 Y. Mao, X. Wang, S. Xia, K. Zhang, C. Wei, S. Bak, Z. Shadike, X. Liu, Y. Yang and R. Xu, *Adv. Funct. Mater.*, 2019, **29**, 1900247.
25 R. Jung, P. Strobl, F. Maglia, C. Stinner and H. A. Gasteiger, *J. Electrochem. Soc.*, 2018, **165**, A2869.
26 R. Jung, M. Metzger, F. Maglia, C. Stinner and H. A. Gasteiger, *J. Phys. Chem. Lett.*, 2017, **8**, 4820–4825.
27 Q. Wang, C.-H. Shen, S.-Y. Shen, Y.-F. Xu, C.-G. Shi, L. Huang, J.-T. Li and S.-G. Sun, *ACS Appl. Mater. Interfaces*, 2017, **9**, 24731–24742.
28 X. Xiao, Z. Xu, D. Hou, Z. Yang and F. Lin, *J. Synchrotron Radiat.*, 2022, **29**, 1085–1094.
29 X. Xiao, Z. Xu, F. Lin and W.-K. Lee, *J. Synchrotron Radiat.*, 2022, **29**, 266–275.
30 M. M. Rahman, K. Xia, X.-Q. Yang, K. Ariyoshi and E. Hu, *Nano Lett.*, 2023, **23**, 7135–7142.
31 A. Leonard, B. Planden, K. Lukow and D. Morrey, *J. Energy Storage*, 2023, **72**, 108422.
32 C. Fang, B. Lu, G. Pawar, M. Zhang, D. Cheng, S. Chen, M. Ceja, J.-M. Doux, H. Musrock and M. Cai, *Nat. Energy*, 2021, **6**, 987–994.